Series Clutched Actuation for Collision Tolerant High-Speed Robots

Frederik Ostyn*
ESME
Ghent University
Ghent, 9000
Core Lab MIRO
Flanders Make
Lommel, 3920
Email: frederik.ostyn@ugent.be

Bram Vanderborght
Robotics and Multibody Mechanics
Vrije Universiteit Brussel
Brussels, 1050
imec
Leuven, 3001
Email: bram.vanderborght@vub.be

Guillaume Crevecoeur
ESME
Ghent University
Ghent, 9000
Core Lab MIRO
Flanders Make
Lommel, 3920
Email: guillaume.crevecoeur@ugent.be

ABSTRACT

Collisions at high speed can severely damage robots with non-backdrivable drivetrains. Adding an overload clutch in series can improve the robot's collision tolerance without compromising its high dynamic performance. This paper aims at determining the speed above which overload clutches are required in a 2-link manipulator arm. Furthermore, the optimal clutch topology as function of the impact velocity is investigated. Thirdly, it is evaluated if adding clutches can lower the impact force on the arm. Finally, the maximum speed is identified below which impact-aware robot control is possible. The latter requires that none of the clutches decouple during an intentional collision with the environment. These answers are obtained through collision simulations and experiments with a custom build two-link arm. It was found that adding a clutch reduces the torque experienced by the drivetrain by an order of magnitude and below the limit momentary peak torque of the strain wave gears that are used. Adding a clutch to the elbow joint of the two-link arm was effective in protecting the shoulder as well if the impact occurred at the tool center point. With respect to a rigid elbow joint, the clutched elbow joint reduced the collision force at the tool by only 8%. To demonstrate that the arm is impact-aware, a box of 8 kg is approached, impacted and pushed at 1 m/s without decoupling a clutch, nor damaging the robot's hardware.

1 Introduction

Robots with non-backdrivable drivetrains may fail when colliding at high speed. Examples are humanoid robots falling over resulting in damaged shoulder actuators [1,2] and high-speed industrial robots colliding with an obstacle [3]. A particular case where the risk for collision increases significantly are Hybrid High-Speed Cobots (HHSCs) that can switch between high-speed (unsafe) and low-speed (collaborative) mode [4–6]. A mistake made by the human operator while in collaborative mode can lead to catastrophic failure of the robot hardware during a collision after switching to high-speed mode. Impact-aware robot control [7] is another case where the robot –now intentionally– experiences impulse loading, e.g. when pushing a box without slowing down or when tossing an object. By operating the robot at the collision tolerance limits, there is a high chance of critical damage to the hardware in case something goes wrong.

*Address all correspondence to this author.

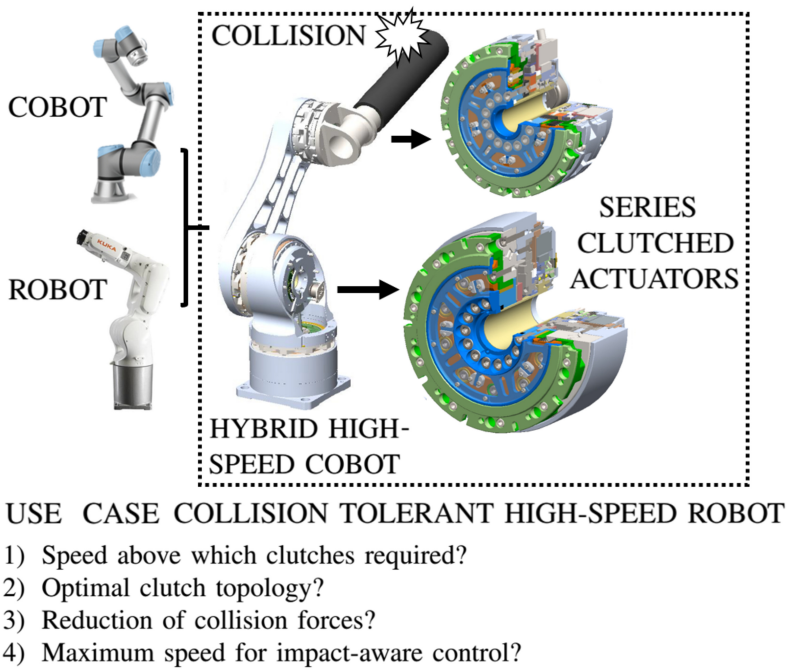

Fig. 1. A Hybrid High-Speed Cobot (HHSC) is capable of switching between high-speed and collaborative mode. It serves as use case for a collision tolerant high-speed robot. A custom three axis HHSC equipped with series clutched actuators is shown. The research questions are listed as well.

Robots with non-backdrivable drivetrains can be protected by adding overload clutches [1–3, 8], classifying as Series Clutched Actuators (SCAs). In contrast to Series Elastic Actuation [9] and compliant links variants [10], they are torsionally stiff in nominal operation, allowing for high dynamic performance. They do not have an additional motor to set the stiffness or operate as agonist–antagonist pair as Variable Stiffness Actuators (VSA, [11,12]) do which reduces the cost of the overload protection.

Most SCA-studies concern safe physical Human Robot Interaction (pHRI) rather than protecting the robot's hardware during high-speed collisions. Examples are the safe joint mechanism SJM-II [13], the Spring-Clutch [14], a friction clutch with variable threshold [15], clutches that allow to switch between passive and active mode [16] or discrete states of compliance [17] and a clutch activated by air cushions [18]. Variants exist that implement clutches in the links as well [19].

Similar modelling and experimental methods developed for pHRI can be used to study how effective SCAs are in protecting the robot's hardware during a high-speed collision. In [15], the collision is modelled as an external static force to derive the optimal threshold that safeguards the operator without decoupling in nominal robot operation. This study was extended in [20] and used to optimally adapt the robot's design in [21]. By modelling the collision as a static force, the complete robot and contact dynamics are neglected. While acceptable in pHRI given the lower speeds, the high-speed collisions discussed in this paper require a dynamic collision model. Such a dynamic model is either non-smooth [22] or continuous [23]. In the former case hard impact is assumed, primarily affecting the inertia term while in the latter model, the robot-environment interaction is represented as a mass-spring-damper system. In [24], three levels of impact abstraction are compared in order to predict the post-impact velocity: (a) compliant contact and flexible robot, both represented by a mass-spring-damper, (b) hard contact and flexible robot and (c) hard contact and rigid robot, corresponding to the non-smooth approach. In case of a KUKA LWR IV+ impacting at speeds up to 0.20 m/s, it was found that (c) already correctly predicts the overall trend while (a) and (b) capture the higher order dynamics. Different methods to calculate the inverse inertia matrix required for the non-smooth approach are compared in [25]. The inverse of the composite-rigid-body inertia transformed at the contact point turned out to be the most accurate. Park *et al.* used mass-spring-damper models to evaluate the collision safety of rigid service robots [26]. Haddadin *et al.* studied the impact decoupling properties of elastic robots as function of joint compliance [27]. Lauzier *et al.* simulated the collision forces in case of a rigid, compliant and clutched actuator with and without covering the robot's links in soft skin [28]. They saw reductions of up to 30-45% in collision force attributed to the clutches in combination with compliant covering.

Using these techniques, this article aims at answering the following research questions:

1. What is the speed above which a clutch is required to avoid damage to the robot's hardware?
2. In which joint(s) is a clutch most effective, or stated otherwise: what is the optimal clutch topology? At least a two-link robot model is required for this purpose (in contrast to [28]).
3. Can the collision forces on the arm and/or tool be reduced if the robot is fitted with multiple clutches?

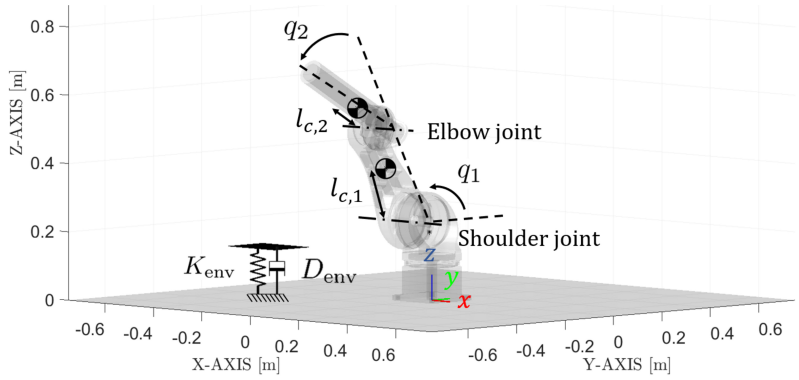

Fig. 2. Robot simulation model showing link positions q_1 and q_2 as well as the environment interaction model.

4. What is the maximum operational range for impact-aware robot control? Stated otherwise: what is the maximum speed below which none of the clutches decouple?

The answers to these questions are the main contributions of this article, validated both in collision simulations as well as experiments with a two-link arm.

Fig. 1 shows the robot that will serve as use case. It is a HHSC with overload clutches that combine the working principles of a standard friction and cam clutch in a single torque dense design [3]. This type of clutch has a unique relative position to return to when de- and recoupling. Secondly, it has sufficient residual torque when decoupled to counteract the robot's gravity and keep it upright. To demonstrate this particular feature, the collision experiments will be executed in the vertical plane, in contrast to e.g. [13]. A version tailored to HHSC with integrated joint torque sensing and clutch decoupling detection was used [29]. In order to take into account delays in detecting and reacting to the collision, a realistic collision detection algorithm such as the bandpass momentum observer [30] as well as a motor controller was implemented.

This article continues with the simulation model in Section 2 which is used to compare the impact forces and torques depending on the clutch topology and robot speed (Section 3). These predictions are experimentally verified in Section 4. The article is concluded in Section 5.

2 Robot and collision model

In this section a collision simulation model is presented, including a two-link clutched robot, the robot-environment interaction model, a collision detection algorithm based on the bandpass momentum observer and the low level motor controller.

2.1 Robot Model with External Load

The robot is modelled as a planar elbow manipulator with link positions $\mathbf{q} = [q_1; q_2]$, link lengths l_1 and l_2, masses m_1 and m_2, positions of the centers of gravity $l_{c,1}$ and $l_{c,2}$ and moment of inertia at these centers of gravity I_1 and I_2 as shown in Fig. 2. The exact values are listed in Table 1. The Euler–Lagrange equations as reduced to the link side read

$$\mathbf{J}_l(\mathbf{q})\ddot{\mathbf{q}} + \mathbf{C}(\mathbf{q},\dot{\mathbf{q}})\dot{\mathbf{q}} + \mathbf{g}(\mathbf{q}) = \boldsymbol{\tau}_{\text{oc}} + \mathbf{J}^T(\mathbf{q})\boldsymbol{\xi}_{\text{ext}} \tag{1}$$

with positive definite inertia matrix $\mathbf{J}_l(\mathbf{q}) \in \mathbb{R}^{2\times2}$, positive semi–definite centrifugal and coreolis terms $\mathbf{C}(\mathbf{q},\dot{\mathbf{q}}) \in \mathbb{R}^{2\times2}$ and gravity term $\mathbf{g}(\mathbf{q}) \in \mathbb{R}^{2\times1}$. Both axes are driven via a series clutched actuator transmitting torque $\boldsymbol{\tau}_{\text{oc}} \in \mathbb{R}^{2\times1}$ and can be subject to an external collision wrench $\boldsymbol{\xi}_{\text{ext}} = [\mathbf{f}_{\text{ext}}; \mathbf{0}_{3\times1}]$ with $\mathbf{f}_{\text{ext}}$ the external force assuming zero external torque. The latter is converted to joint torque $\boldsymbol{\tau}_{\text{ext}} = \mathbf{J}^T(\mathbf{q})\boldsymbol{\xi}_{\text{ext}}$ via Jacobian $\mathbf{J}(\mathbf{q})$. Expressions for $\mathbf{J}_l(\mathbf{q}), \mathbf{C}(\dot{\mathbf{q}},\mathbf{q}), \mathbf{g}(\mathbf{q})$ and $\mathbf{J}(\mathbf{q})$ were derived a.o. in [31]. The Jacobian reads:

$$\mathbf{J}(\mathbf{q}) = \begin{bmatrix} 0 & 0 \\ -l_1 s_{q_1} - l_2 s_{q_1+q_2} & -l_2 s_{q_1+q_2} \\ l_1 c_{q_1} + l_2 c_{q_1+q_2} & l_2 c_{q_1+q_2} \\ 1 & 1 \\ 0 & 0 \\ 0 & 0 \end{bmatrix} \tag{2}$$

Table 1. Robot model and collision simulation parameters.

Specification/parameter	Symbol	Unit	Value
Link length 1	l_1	mm	325
Link length 2	l_2	mm	375
Mass link 1	m_1	kg	8.7
Mass link 2	m_2	kg	4.5
Center of gravity	$l_{c,1}$	mm	152
Center of gravity	$l_{c,2}$	mm	65
Moment of inertia link 1	I_1	kgm^2	0.220
Moment of inertia link 2	I_2	kgm^2	0.062
Stiffness rigid drivetrain 2	$k_{\mathrm{r},2}$	Nm/rad	2×10^7
Stiffness unclutched drivetrain 1	$k_{\mathrm{hd},1}$	Nm/rad	8.8×10^4
Stiffness unclutched drivetrain 2	$k_{\mathrm{hd},2}$	Nm/rad	4.7×10^4
Stiffness clutched drivetrain 1	$k_{\mathrm{oc},1}$	Nm/rad	4.2×10^4
Stiffness clutched drivetrain 2	$k_{\mathrm{oc},2}$	Nm/rad	3.0×10^4
Damping drivetrain 1	d_1	Nms/rad	25
Damping drivetrain 2	d_2	Nms/rad	10
Clutch threshold 1	$\tau_{\mathrm{th},1}$	Nm	240
Clutch threshold 2	$\tau_{\mathrm{th},2}$	Nm	90
Clutch residual torque 1	$\tau_{\mathrm{res},1}$	Nm	60
Clutch residual torque 2	$\tau_{\mathrm{res},2}$	Nm	30
Coulomb friction motor 1	$\tau_{C,1}$	Nm	50
Coulomb friction motor 2	$\tau_{C,2}$	Nm	25
Viscous friction motor 1	D_1	Nms/rad	5
Viscous friction motor 2	D_2	Nms/rad	2.5
Environment stiffness	K_{env}	N/m	3.5×10^5
Environment damping	D_{env}	Ns/m	6×10^2
Mom. obs. low-pass gain 1	$K_{L,1}$	rad/s	500
Mom. obs. low-pass gain 2	$K_{L,2}$	rad/s	500
Mom. obs. high-pass gain 1	$K_{H,1}$	rad/s	100
Mom. obs. high-pass gain 2	$K_{H,2}$	rad/s	100
Collision detection threshold 1	$\tau_{\mathrm{col},1}$	Nm	30
Collision detection threshold 2	$\tau_{\mathrm{col},2}$	Nm	10
Position control gain	K_v	1/s	1.0
Velocity control gain	K_p	Nms/rad	0.1
Velocity control integrator gain	T_i	s	0.1

if the collision occurs in the Tool Center Point (TCP) with s_* and c_* shorthand for $\sin(*)$ and $\cos(*)$ respectively. The elements of the link inertia matrix $\mathbf{J}_l(\mathbf{q})$ can be derived as

$$\begin{aligned} J_{l,11} &= m_1 l_{c,1}^2 + m_2(l_1^2 + l_{c,2}^2 + 2l_1 l_{c,2} c_{q_2}) + I_1 + I_2 \\ J_{l,12} &= J_{l,21} = m_2(l_{c,2}^2 + l_1 l_{c,2} c_{q_2}) + I_2 \\ J_{l,22} &= m_2 l_{c,2}^2 + I_2 \end{aligned} \tag{3}$$

The gravity term reads

$$\mathbf{g}(\mathbf{q}) = \begin{bmatrix} (m_1 l_{c,1} + m_2 l_1) g c_{q_1} + m_2 l_{c,2} g c_{q_1+q_2} \\ m_2 l_{c,2} g c_{q_1+q_2} \end{bmatrix} \tag{4}$$

and $\mathbf{C}(\mathbf{q},\dot{\mathbf{q}})$ is given by

$$\mathbf{C}(\mathbf{q},\dot{\mathbf{q}}) = -m_2 l_1 l_{c,2} s_{q_2} \begin{bmatrix} \dot{q}_2 & \dot{q}_1 + \dot{q}_2 \\ -\dot{q}_1 & 0 \end{bmatrix} \tag{5}$$

2.2 Series Clutched Actuator Model

The dynamics of the motor side (reduced to the link side) are modelled as

$$\mathbf{J}_m\ddot{\boldsymbol{\theta}} = \boldsymbol{\tau}_m - \boldsymbol{\tau}_f - \boldsymbol{\tau}_{\text{oc}} \tag{6}$$

with constant motor inertia matrix $\mathbf{J}_m = \text{diag}(\text{J}_{\text{m},1}, \text{J}_{\text{m},2}) \in \mathbb{R}^{2\times 2}$, driven by the motor torque $\boldsymbol{\tau}_m = [\tau_{m,1}; \tau_{m,2}]$, a friction torque $\boldsymbol{\tau}_f = [\tau_{f,1}; \tau_{f,2}]$ with components

$$\tau_{f,i} = D_i\dot{\theta}_i + \begin{cases} \frac{\dot{\theta}_i}{\varepsilon}\min(|\theta_i|, \tau_{C,i}) & \text{if } |\dot{\theta}_i| \leqslant \varepsilon \\ \text{sign}(\dot{\theta}_i)\tau_{C,i} & \text{otherwise} \end{cases} \tag{7}$$

with D_i the viscous friction coefficient [Nm/(rad/s)], $\tau_{C,i}$ the Coulomb term [Nm] and with $\varepsilon = 0.01$ rad/s introduced for computational purposes [32]. Each component of the clutch torque $\boldsymbol{\tau}_{\text{oc}}$ satisfies

$$\tau_{\text{oc,i}} = \begin{cases} k_i\Delta q_i + d_i\Delta\dot{q}_i & \text{if } |k_i\Delta q_i + d_i\Delta\dot{q}_i| \leqslant \tau_{\text{th,i}} \\ \frac{\Delta\dot{q}_i}{\varepsilon}\tau_{\text{res,i}} & \text{if } |...| > \tau_{\text{th,i}} \text{ and } \Delta\dot{q}_i \leqslant \varepsilon \\ \text{sign}(\Delta\dot{q}_i)\tau_{\text{res,i}} & \text{otherwise} \end{cases} \tag{8}$$

with k_i, d_i respectively the i^{th} drivetrain stiffness and damping of the strainwave gear and clutch in series, with $\Delta q_i := \theta_i - q_i$, with $\tau_{\text{th,i}}$ the clutch threshold torque and $\tau_{\text{res,i}}$ the residual torque. If the transmitted torque is larger (in absolute value) than the threshold torque $\tau_{\text{th,i}}$, the clutch decouples and transmits maximally the residual torque $\tau_{\text{res,i}} < \tau_{\text{th,i}}$. Without clutch, $\tau_{\text{oc,i}}$ is to be replaced by $\tau_{\text{hd,i}} = k_{\text{hd,i}}\Delta q_i + d_{\text{hd,i}}\Delta\dot{q}_i$ where $k_{\text{hd,i}}$ and $d_{\text{hd,i}}$ are only due to the strainwave gear. In case the connection of joint i is rigid, θ_i is fixed and $\ddot{\theta}_i = \dot{\theta}_i = 0$. The torque $\tau_{\text{oc,i}}$ is to be replaced by $\tau_{\text{r,i}} = k_{r,i}\Delta q_i - d_{r,i}\dot{q}_i$ where $k_{r,i}$ and $d_{r,i}$ are due to the rigid coupling. The i^{th} joint motor dynamics, represented by Eq. (6), reduces to $\tau_{m,i} = \tau_{\text{oc,i}}$. Concerning the dampening, it is assumed that $d_i = d_{\text{hd,i}} = d_{r,i}$. Again, ε is introduced to avoid chatter at near-zero speeds.

2.3 Environment Interaction Model

The interaction with the environment is modelled as a spring-damper [23]. A collision is assumed to happen as soon as the arm is below the horizontal plane intersecting the shoulder joint axis:

$$f_{\text{ext,3}} = \begin{cases} -K_{\text{env}}(z - z_{\text{col}}) - D_{\text{env}}\dot{z} & \text{if } z \leqslant z_{\text{col}} \\ 0 & \text{otherwise} \end{cases} \tag{9}$$

with z the vertical robot position in Cartesian coordinates in task space and K_{env} and D_{env} the stiffness and damping respectively.

2.4 Collision Detection and Reaction

The bandpass momentum observer boils down to low- and high-pass filtering the (unknown) external torque $\boldsymbol{\tau}_{\text{ext}}$ which in the Laplace domain reads

$$\hat{\tau}_{\text{ext,i}} = \underbrace{\frac{s}{s + K_{H,i}}}_{\text{HPF}}\underbrace{\frac{K_{L,i}}{s + K_{L,i}}}_{\text{LPF}}\tau_{\text{ext,i}} \tag{10}$$

for each of its components $\hat{\tau}_{\text{ext,i}}$. In time domain and after integrating twice, one gets [30]:

$$\begin{aligned} \hat{\tau}_{\text{ext,i}} &= K_{L,i}\left[p_i(t) - p_i(0)\right] \\ &\quad - K_{L,i}\int_0^t \left[\tau_{\text{oc,i}} - \beta_i(\mathbf{q}, \dot{\mathbf{q}}) + (1 + \frac{K_{H,i}}{K_{L,i}})\hat{\tau}_{\text{ext,i}}\right] dt \\ &\quad - K_{L,i}K_{H,i}\int_0^t \left[\int_0^t \hat{\tau}_{\text{ext,i}} dt\right] dt \end{aligned} \tag{11}$$

where $\boldsymbol{\beta}(\mathbf{q},\dot{\mathbf{q}})$ is defined as

$$\boldsymbol{\beta}(\mathbf{q},\dot{\mathbf{q}}) = \mathbf{g}(\mathbf{q}) - \mathbf{C}^T(\mathbf{q},\dot{\mathbf{q}})\dot{\mathbf{q}} \tag{12}$$

which can be evaluated explicitly:

$$\boldsymbol{\beta} = \begin{bmatrix} (m_1 l_{c,1} + m_2 l_1) g c_{q_1} + m_2 l_{c,2} g c_{q_1+q_2} \\ m_2 l_1 l_{c,2} c_{q_1+q_2} + m_2 l_1 l_{c,2} s_{q_2} \dot{q}_1 (\dot{q}_1 + \dot{q}_2) \end{bmatrix} \tag{13}$$

given the analytical expressions for the gravity term $\mathbf{g}(\mathbf{q})$ and the centrifugal and coreolis matrix $\mathbf{C}(\mathbf{q},\dot{\mathbf{q}})$. The moment $\mathbf{p}$ is defined as $\mathbf{p} = \mathbf{J}_l\dot{\mathbf{q}}$. If $K_{H,i} = 0$ is chosen, one obtains the standard momentum observer $\hat{\boldsymbol{\tau}}^*_{\text{ext}}$ which acts as a low-pass filter for the external torque $\boldsymbol{\tau}_{\text{ext}}$.

The link position $\mathbf{q}$ and velocity $\dot{\mathbf{q}}$ are estimated based on the motor position $\boldsymbol{\theta}$ and the overload clutch torque $\boldsymbol{\tau}_{\text{oc}}$ via $q_i \approx \theta_i - \tau_{\text{oc,i}}/k_i$ assuming steady state. Note that the latter equation is only valid if the clutch is coupled. Given the transient nature of the impact, this assumption may also not be valid during the collision. This may lead to an imprecise estimate of the external load during the impact. We assume however that this estimate does exceed the collision threshold so that the impact is correctly detected.

A collision is detected by comparing the absolute value of the bandpass momentum observer with a predefined collision threshold: $|\hat{\tau}_{\text{ext,i}}| > \tau_{\text{col,i}}$ signals a collision of actuator i. The robot is instructed to stop as fast as possible.

2.5 Low Level Control

Each motor torque $\tau_{m,i}$ is given by

$$\tau_{m,i} = \begin{cases} \tau_{c,i} & \text{if } |\tau_{c,i}| \leqslant \tau_{\text{sat,i}} \\ \text{sign}(\tau_{c,i})\tau_{\text{sat,i}} & \text{otherwise} \end{cases} \tag{14}$$

with

$$\tau_{c,i} = K_p(K_v + \frac{1}{T_i})(q_{\text{des,i}} - q_i) + K_p(\dot{q}_{\text{des,i}} - \dot{q}_i) + \frac{K_p K_v}{T_i}\int (q_{\text{des,i}} - q_i)dt \tag{15}$$

which is a standard PID–controller based on a cascaded velocity and position controller with $\tau_{\text{sat,i}}$ the maximum torque of motor i, chosen equal to the clutch threshold torque $\tau_{\text{th,i}}$. K_p, K_v and T_i are tuning parameters and $q_{\text{des,i}}$ the desired motor position.

3 Collision simulations

The collision simulation model derived in the previous section is used to determine the robot velocity above which overload protection is required. It is furthermore determined what the optimal clutch topology is by varying if a joint is fitted with a clutch or not.

3.1 Optimal Clutch Topology

Fig. 3 shows the collision simulation in case of (a) an unclutched shoulder with stiff rigid elbow, (b) a clutched shoulder with rigid elbow, (c) an unclutched shoulder and elbow, (d) with clutched shoulder and unclutched elbow and (e) with clutches both in the shoulder and elbow. Each time, the shoulder and elbow motor position is shown, as well as the difference between motor and load side position, their speeds, the motor torque, the clutch torque along with their maximum ratings and the collision force as measured at the point of collision.

In the first two simulations, the elbow is assumed rigid as if the robot has only a single link. This is modelled by setting the stiffness of the elbow to $k_{r,2} = 2 \times 10^7$ Nm/rad, matching the torsional stiffness of the dummy actuator used in the experiments to follow. The results are shown in Fig. 3 (a) and (b) for the unclutched and clutched case respectively. Only the simulation with clutched shoulder will be experimentally verified (see Section 4) as the former indicates overloading of the actuator's drivetrain. By adding the clutch, the shoulder is effectively protected as the clutch torque $\tau_{\text{oc,1}}$ is lower than the maximum allowed instantaneous torque of the strainwave gear. No significant reduction in collision force is observed however.

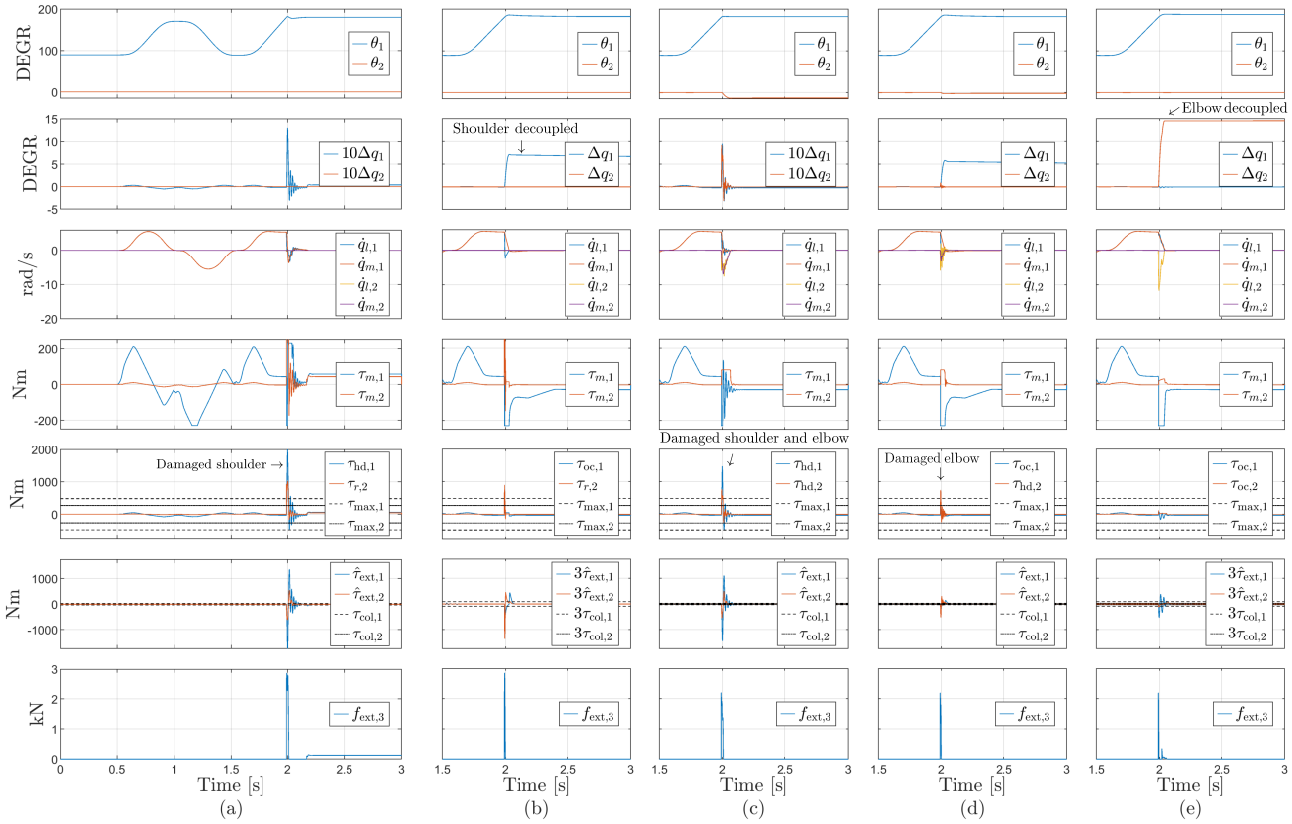

Fig. 3. Collision simulation with (a) unclutched shoulder and stiff rigid elbow; (b) clutched shoulder and rigid elbow; (c) unclutched shoulder and elbow, (d) clutched shoulder and unclutched elbow and (e) clutched shoulder and elbow.

If the rigid connection between upper and lower arm is replaced by an unclutched actuator, the impact force amplitude reduces by 20% as shown in Fig. 3(c). The latter can be attributed to the actuator's inherent compliance, in particular the harmonic drive compliance. It acts as a mechanical low pass filter and decouples the motor side inertia during a high-speed collision. The reduction in collision force is overshadowed by the excessive loading of the harmonic drives $\tau_{oc,1}$ and $\tau_{oc,2}$. Overload protection is hence required if catastrophic failure of (both) drivetrains is to be avoided. The question is now which clutch topology is best suited. Three options exist: a single overload clutch in either elbow (1) or shoulder (2) or clutches in both actuators (3).

If only the shoulder is overload protected, the simulation shown in Fig. 3(d) predicts catastrophic damage to the elbow. The simulations with unclutched shoulder and clutched elbow gave similar results as with both joints clutched. The latter simulation is shown in Fig. 3(e). The elbow clutch allows the arm to kink (as indicated by $\theta_2 - q_2 \approx 15^\circ$) and hinge about the elbow joint, reducing the inertia to be slowed down fast. Both clutch torques $\tau_{oc,1..2}$ are below their maximum ratings and only the elbow clutch decoupled ($\tau_{oc,1} < \tau_{th,1}$). Adding a clutch in the elbow hence protects both the shoulder and elbow actuator. Note however that the shoulder is not protected if the collision occurs at the upper arm of the robot. In order to protect both the elbow and shoulder in all situations, two clutches are required. Similar to the case with rigid elbow, the clutch does not significantly reduce the maximum collision force at the point of impact.

3.2 Influence Of Robot Speed

The collision simulations up to now gave insight in how the shoulder and elbow joint drivetrains can be protected during a collision at high speed. In this section, it is investigated from which speed on overload protection is required.

Fig. 4 shows the torques $\tau_{oc,1..2}$ as function of speed at the tool center point and clutch topology: no clutches on shoulder and elbow versus both shoulder and elbow have an overload clutch. Also shown are the maximum repeatable torques of the strainwave gears as well as the clutch threshold torques $\tau_{th,1..2}$. Note that the threshold torques could be chosen differently (as long as they are below the maximum repeatable torques of the strainwave gear). They were chosen slightly lower than the maximum rated torque of the strainwave gear as this allows to decouple the clutch with the actuator itself which proved handy during testing and calibration. Moreover, the chosen clutch threshold torques were found high enough to demonstrate impact-aware robot control as will be discussed in the experimental section (Section 4).

Note that with increasing speed, the elbow joint is the first to be overloaded if not fitted with a clutch. Another important

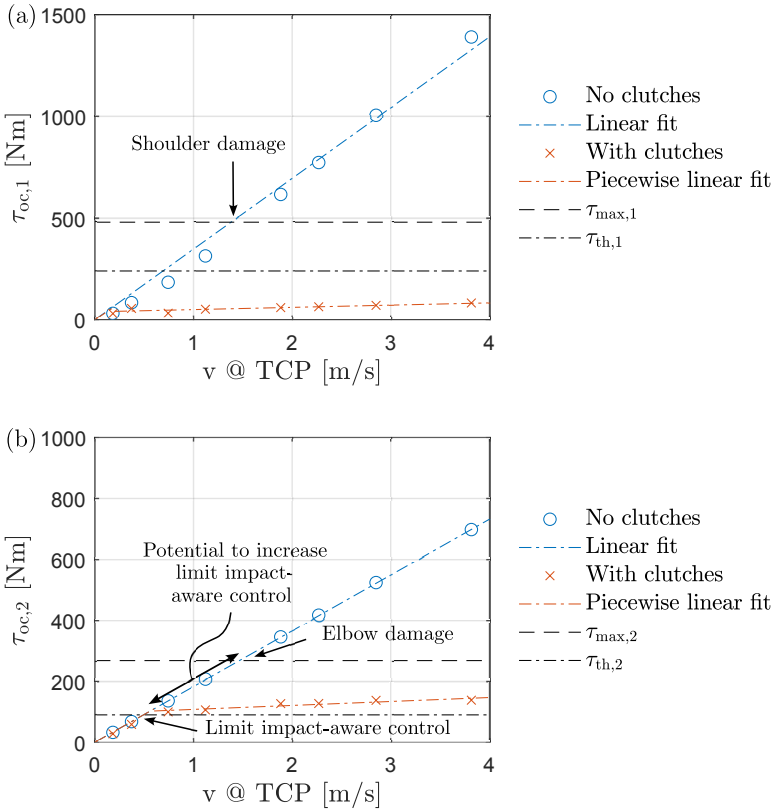

Fig. 4. Influence of robot speed and clutch topology on the shoulder (a) and elbow (b) joint torque. These graphs allow to determine two important metrics: (1) the speed above which overload protection is required and (2) the maximum speed that allows impact-aware robot control for a robot with series clutched actuators.

speed limit is the maximum velocity at which none of the clutches decouple during impact. This is the region that allows for impact-aware robot control. More concretely, this is the maximum speed where the joint torques do not exceed their respective clutch thresholds $\tau_{th,1}$ and $\tau_{th,2}$. Figure 4 shows that this threshold is reached first in the elbow joint. The associated velocity is hence the maximum velocity for impact-aware control. When programming conventional robots without overload clutches, impacts are typically avoided, e.g. by slowly approaching objects. Given the assurance of the overload clutches, programming can be altered to allow impacts as long as they are within the impact-aware region. If the impact is too severe and decouples a clutch, it suffices to reset the collision-tolerant robot where a conventional robot without overload protection may have broken down.

4 Experimental validation

4.1 Experimental Setup

The experimental setup shown in Fig. 5 consists of a custom 3-link hybrid high-speed cobot prototype of which the shoulder and elbow joint are used in this study. The shoulder and elbow actuators are respectively driven by Tecnotion QTR-133-25 and QTR-105-25 permanent magnet synchronous motors, CSD-40-50-BB and CSD-32-50-BB harmonic drives and have RLS Aksim-2 absolute magnetic encoders with 20 bit resolution. The complete setup is controlled via a Beckhoff IPC running TwinCAT 3. The overload clutches have integrated capacitive joint torque sensors and clutch decoupling detection, as shown in Figure 6.

4.1.1 Combined Friction Cam Clutch

Figure 6(a–d) respectively show the working principle (a-b) and actual design of the clutch (c-d). An output flange (1) is connected to the robot arm and an input flange (2) connected to the drivetrain. Spring plate (3) is pushed by springs (4) in the recesses of (2), locking both flanges via a form closure (cam). The same set of springs is used to generate an additional force closure through friction between (1) and (2) as well as (2) and (3). If the collision force exceeds the clutch threshold $\tau > \tau_{th}$, the clutch decouples. Sufficient residual torque τ_{res} remains to counteract gravity. Due to the cam, a unique relative position of the input and output flanges exists avoiding recalibration of the robot after recoupling the clutch. More details can be found in [3].

Fig. 5. Snap shots of a collision experiment with a two degrees-of-freedom arm including a shoulder and elbow joint. The different stages are (a) prior to experiment; (b) high-speed motion; (c) collision; (d) kinked arm with decoupled elbow; (e) reset position of the elbow; (f) reset position of the shoulder; (g) fully reset robot; (h) resumed operation.

4.1.2 Integrated Sensing

The input flange (2) is made compliant, represented by torsion spring (6). An electrode (5) is mechanically fixed (but electrically isolated) to one halve. The change in capacitance $C_{\mathrm{JTS}} \uparrow\downarrow$ is related to the torque transmitted by the clutch. A capacitance drop $C_{\mathrm{DEC}} \downarrow$ signals clutch decoupling. The actual implementation (Fig. 6(c-d)) resembles a spoked (7) wheel with four paired electrodes (5) facing several protrusions (8). The use of paired electrodes allows to distinguish between joint torque sensing and clutch decoupling detection. More details can be found in [29]. The capacitive measurement via electrode i, calibrated to represent joint torque if $\tau < \tau_{\mathrm{th}}$, is referenced as $\tau_{\mathrm{cdc,i}}$ in what follows.

4.2 Collision Experiment With Clutched Shoulder And Rigid Versus Clutched Elbow

Fig. 5 shows the different stages of the collision experiments that will be discussed next. All stages are present in an experiment with clutched elbow. Only (a)–(c) and (f)–(h) occur during a collision with a rigid elbow. Fig. 5 (a) shows the robot prior to the experiment; (b) while performing a high-speed motion; (c) at the collision; (d) decoupling of the elbow resulting in a kinked arm; (e) reset position of the elbow; (f) reset position of the shoulder; (g) ready to resume operation and (h) high-speed motion. The different stages are also indicated in the measurements of Figs. 7 and 8.

4.2.1 Collision Experiment With Clutched Shoulder And Rigid Elbow

A first experiment is performed with clutched shoulder and rigid elbow. The robot is hence reduced to a single degree-of-freedom arm. The experiment resembles the collision test reported in [3] although the load inertia differs. The actuator is instructed to move the arm back and forth at high speed, resulting in a collision in the second pass. Fig. 7 shows the shoulder's motor position $\theta_{m,1}$, speed $\dot{\theta}_{m,1}$ and torque $\tau_{m,1}$ as well as the joint torque sensor $\tau_{\mathrm{oc},1}$ readings based on the individual CDC readings $\tau_{\mathrm{cdc},1:1..8}$, the standard and bandpass momentum observer, $\hat{\tau}^{*}_{\mathrm{ext}}$ and $\hat{\tau}_{\mathrm{ext}}$ respectively as well as the collision threshold $\tau_{\mathrm{col},1}$ and the reading of the loadcell with which the arm collides. The collision is detected as the bandpass momentum observer exceeds a predefined threshold. Given the high speed, the overload clutch decouples. This results in diverging CDC readings of the paired electrodes $\tau_{\mathrm{cdc},1:1..8}$ used in the integrated joint torque sensor. By decoupling, the clutch effectively protects the drivetrain as the collision force measured by the load cell would have likely resulted in catastrophic failure of the strainwave gear. In decoupled state, the clutch allows to transfer sufficient residual torque to keep the arm upright and move it at low speed towards a reset point. The shoulder clutch is recoupled allowing to resume its high-speed operation. The measured collision force matches the prediction by the simulation, as shown in Fig. 3(b).

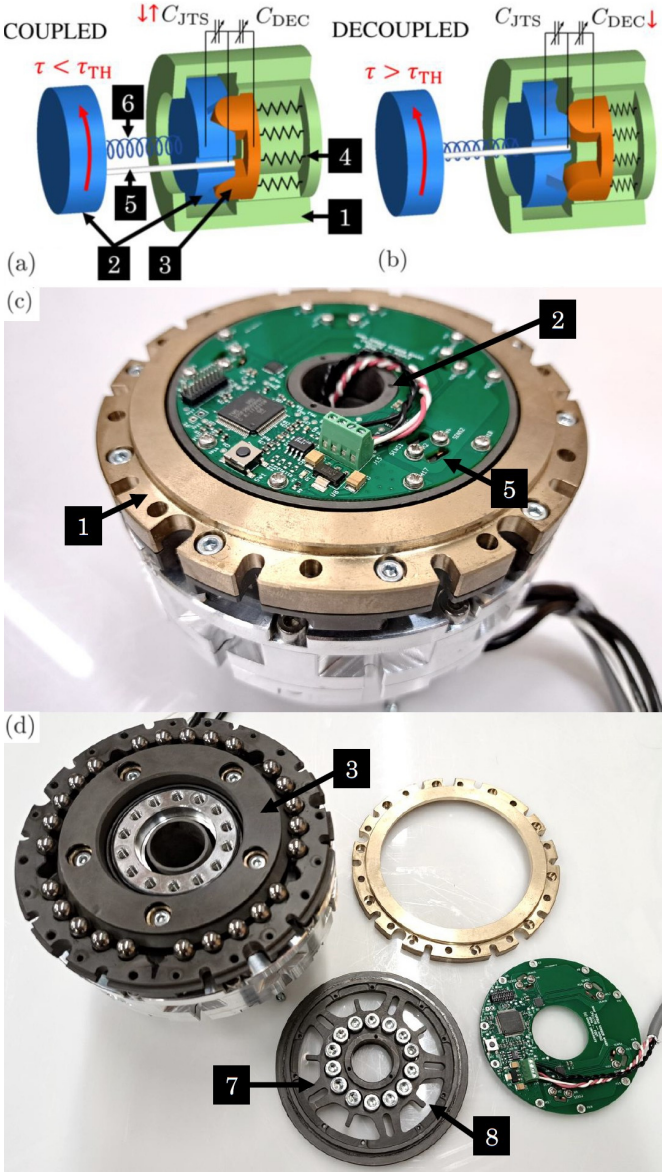

Fig. 6. Working principle (a-b) and actual design (c-d) of the Combined Friction Cam Clutch with integrated joint torque sensing and clutch decoupling detection. Details can be found in the main text.

4.2.2 Collision experiment with clutched shoulder and elbow

In a second experiment, the rigid elbow is replaced by a clutched actuator. The experiment is repeated, resulting in the measurements of Fig. 8. Now the motor position $\boldsymbol{\theta}$, speed $\dot{\boldsymbol{\theta}}$ and torque $\boldsymbol{\tau}_m$ are shown for both the shoulder and the elbow as well as their joint torque sensor readings $\boldsymbol{\tau}_{\mathrm{oc}}$. The elbow (bandpass) momentum observer $\hat{\tau}_{\mathrm{ext},2}$ and the collision threshold $\tau_{\mathrm{col},2}$ are also given, as well as the loadcell reading. Only the elbow joint decouples in this experiment.

Without the clutch the elbow actuator would likely be catastrophically damaged. The elbow clutch does also protect the shoulder joint. By decoupling, the arm is allowed to kink at the elbow, increasing the braking distance of the lower arm. Stated otherwise, by reducing the inertia that must be slowed down fast, the collision load on the shoulder is lowered and the shoulder clutch is not decoupled. The collision force measured by the loadcell is lowered by 8%, which is slightly lower than the 20% predicted by the simulations of Fig. 3(b) versus (e).

4.3 Impact aware pushing of a box

Given the fact that the robot is protected during a high-speed collision, the robot can be used to perform tasks that are (too) risky to try with conventional robots without overload clutches. An example is shown in Fig. 9. A box weighing 8 kg is pushed by the robot. The conventional approach would be to approach the box slowly and gently establish contact prior to pushing the box while monitoring the load of each actuator. In this experiment, the robot moves at high-speed, does not slow

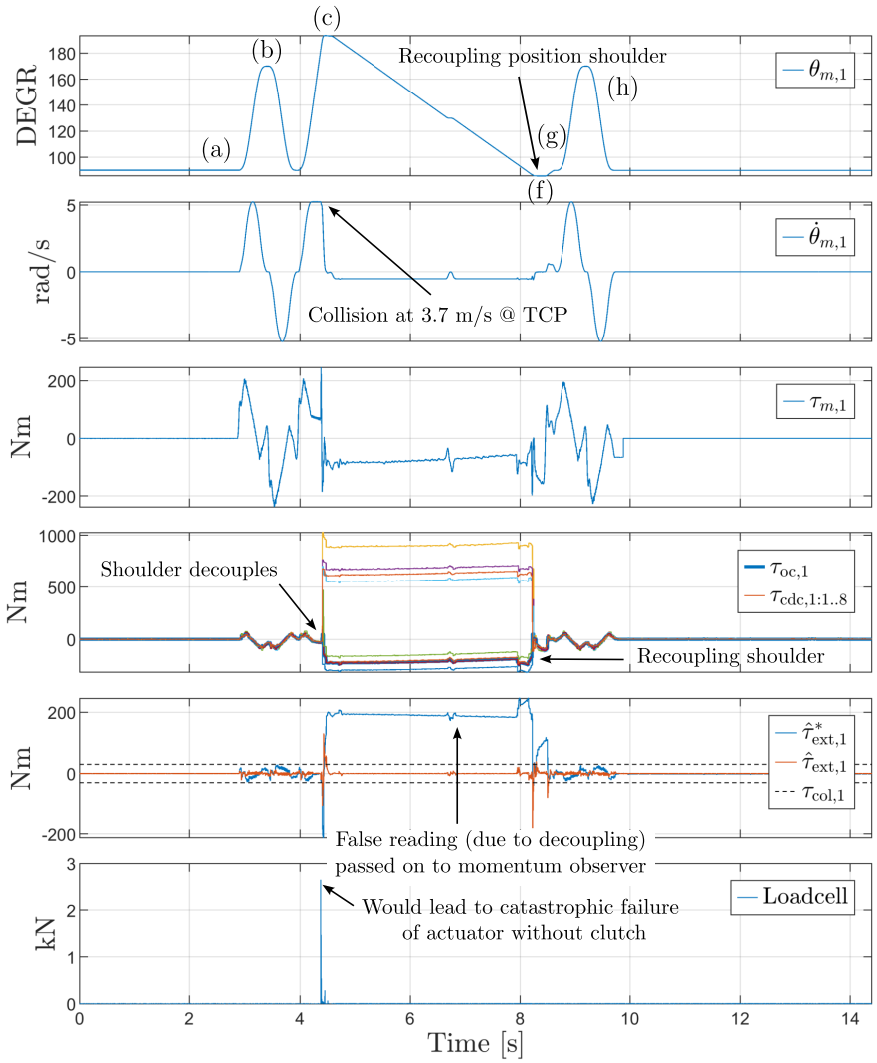

Fig. 7. Shoulder position, speed, motor and load side torque as well as (bandpass) momentum observed load torque and loadcell reading during a collision experiment with clutched shoulder and rigid elbow.

down while establishing contact and pushes the box in a fluent motion. This is an example of impact-aware robot control as introduced in e.g [7], [24] and [25]. It allows to operate at higher speeds, without losing time decelerating to impact the box at near-zero speed. This technology hence makes industrial robots more productive.

Fig. 10 shows the corresponding measurements of the shoulder and elbow motor position $\boldsymbol{\theta}$, speed $\dot{\boldsymbol{\theta}}$, motor $\boldsymbol{\tau}_m$ and joint torque $\boldsymbol{\tau}_{\text{oc}}$ as well as the bandpass momentum observer $\hat{\tau}_{\text{ext},2}$ and the collision threshold $\tau_{\text{col},2}$. Note that the collision detection is ignored in this experiment. The horizontal speed in task space can be calculated as the absolute value of the second component of the screw $\mathbf{J}(\mathbf{q})\dot{\mathbf{q}}$, more concretely

$$|\dot{y}| = |(-l_1 s_{q_1} - l_2 s_{q_1+q_2})\dot{q}_1 - l_2 s_{q_1+q_2}\dot{q}_2| \tag{16}$$

and is as high as 1 m/s at impact. The load torque as measured by the joint torque sensors in the shoulder and elbow is lower than the respective clutch threshold. Neither of the clutches decouple and hence no reset procedure is required. This operation is thus within the bounds of impact-aware operation. Note that the kinematic configuration is different with respect to the collision experiments of Fig. 4. Moreover the stiffness of the box will be lower than that of the table and loadcell.

5 Conclusion

Collisions at high speed can severely damage robots with non-backdrivable drivetrains. This article identified the speed above which an overload clutch is required to protect the drivetrain of a two degrees-of-freedom robot arm. Regarding the

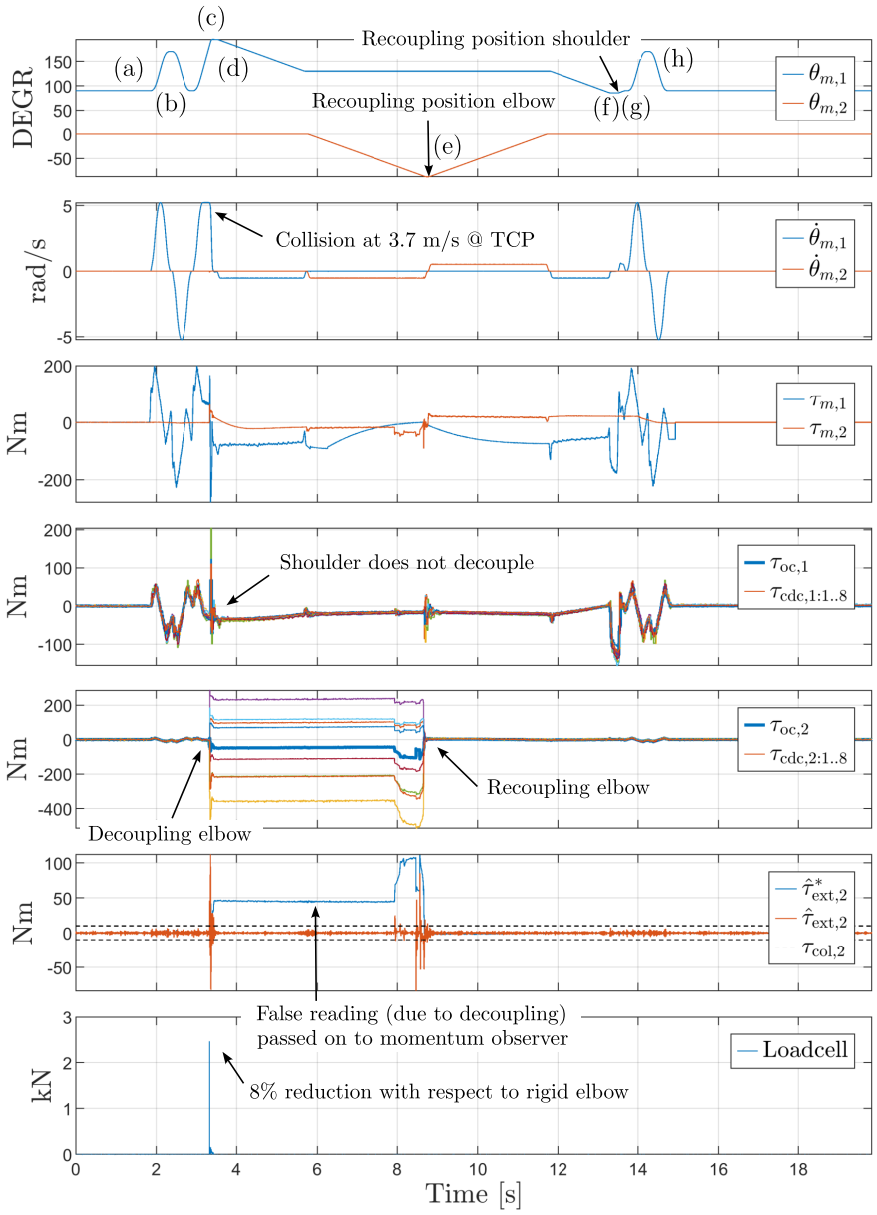

Fig. 8. Shoulder and elbow position, speed, motor and load side torque as well as (bandpass) momentum observed load torque and loadcell reading during a collision experiment with clutched shoulder and elbow.

optimal clutch topology, it was found that adding an overload clutch in the elbow is effective in protecting both the shoulder and elbow joints if the collision occurs at the tool center point. While adding a clutch reduces the drivetrain load considerably, the force at the point of impact does not. The maximum speed below which none of the clutches decoupled was identified as the limit to practise impact-aware robot control. An experiment where a box of 8 kg was pushed at 1 m/s demonstrates how clutch protected robots can be used in scenarios requiring intentional collisions, without having to worry about accidentally damaging the robot's hardware.

Future work will be to extend this analysis to robots with higher degrees of freedom, where the collision force is expected to significantly depend on the robot pose. Other work will focus on the long term performance of the clutch. Especially the positioning accuracy after decoupling multiple times will be evaluated.

Acknowledgements

This work was supported by the Research Foundation - Flanders (FWO) under Grant G0A9623N.

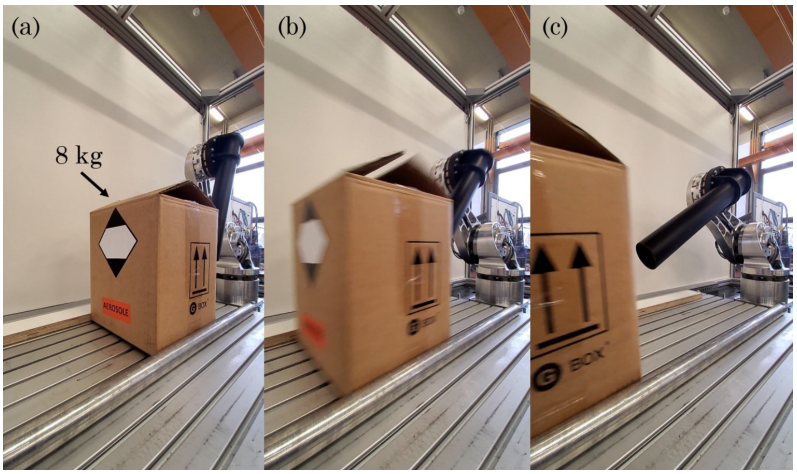

Fig. 9. Snap shots of an impact-aware control experiment. A box of 8 kg is pushed by the robot without decelerating during the approach phase.

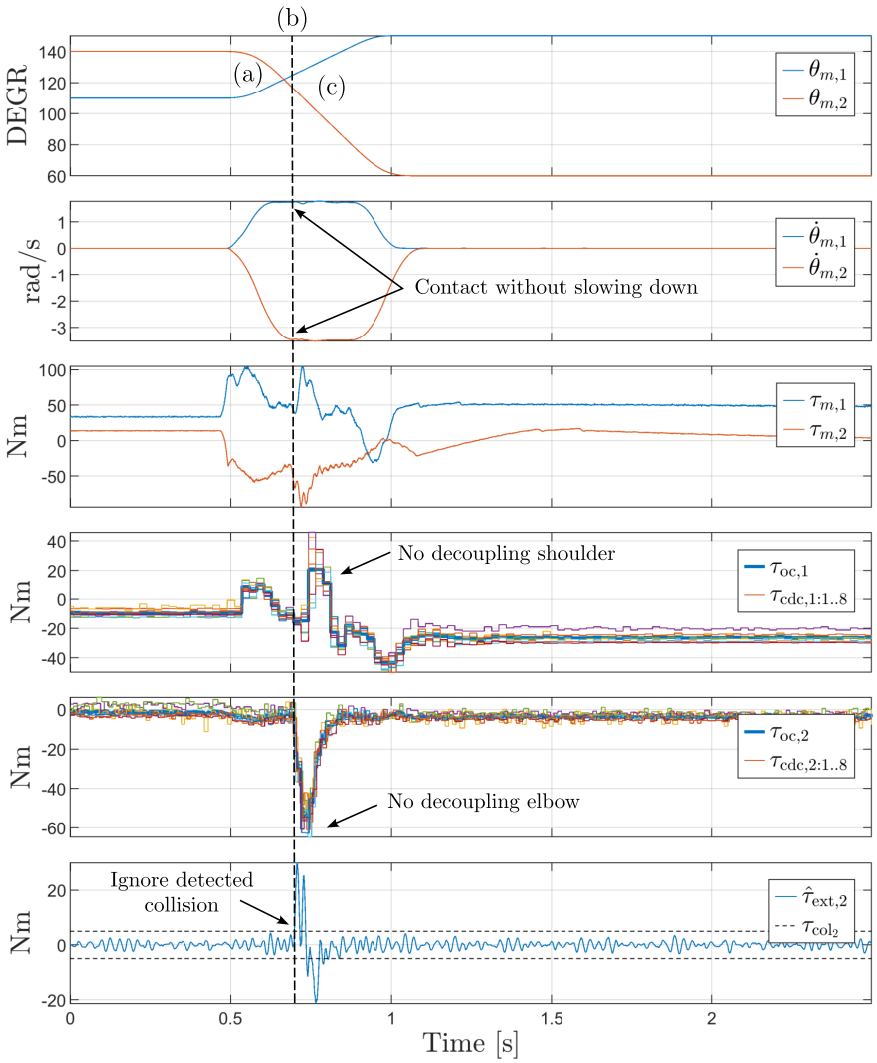

Fig. 10. Shoulder and elbow position, speed, motor and load torque when pushing an 8 kg box without decelerating during the approach phase.

References

[1] Guo, X., Zhang, W., Liu, H., Yu, Z., Zhang, W., and Conus, W., 2015. "A torque limiter for safe joint applied to humanoid robots against falling damage". In 2015 IEEE International Conference on Robotics and Biomimetics (ROBIO), pp. 2454–2459.

[2] Kang, R., Liu, H., Meng, F., Zhang, R., Ma, X., Liu, B., Ming, A., and Huang, Q., 2018. "An overload protector inspired by joint dislocation and reduction for shoulder of humanoid robot". In 2018 IEEE International Conference on Robotics and Biomimetics (ROBIO), pp. 2019–2024.

[3] Ostyn, F., Lefebvre, T., Vanderborght, B., and Crevecoeur, G., 2021. "Overload clutch design for collision tolerant high–speed industrial robots". *IEEE Robotics and Automation Letters,* **6**(2), pp. 863–870.

[4] ABB Swifty. https://new.abb.com/products/robotics/robots/collaborative-robots/swifti. Accessed: 26.08.2022.

[5] Yaskawa HC20DTP. https://www.motoman.com. Accessed: 26.08.2022.

[6] Comau Racer-5-0.80 Cobot. https://www.comau.com. Accessed: 26.08.2022.

[7] van Steen, J. J., van de Wouw, N., and Saccon, A., 2022. "Robot control for simultaneous impact tasks via quadratic programming-based reference spreading". pp. 3865–3872.

[8] Baek, S., Moon, H., Choi, H., and Koo, J., 2021. "A new cam-follower safety joint mechanism design based on variable-length four-bar linkage for robot safety". *Journal of Mechanisms and Robotics,* **14**, p. 011004.

[9] Tsagarakis, N. G., Laffranchi, M., Vanderborght, B., and Caldwell, D. G., 2009. "A compact soft actuator unit for small scale human friendly robots". In 2009 IEEE International Conference on Robotics and Automation, pp. 4356–4362.

[10] She, Y., Su, H.-J., Meng, D., Song, S., and Wang, J., 2018. "Design and modeling of a compliant link for inherently safe corobots". *Journal of Mechanisms and Robotics,* **10**, p. 011001.

[11] Vanderborght, B., Albu-Schaeffer, A., Bicchi, A., Burdet, E., Caldwell, D., Carloni, R., Catalano, M., Eiberger, O., Friedl, W., Ganesh, G., Garabini, M., Grebenstein, M., Grioli, G., Haddadin, S., Hoppner, H., Jafari, A., Laffranchi, M., Lefeber, D., Petit, F., Stramigioli, S., Tsagarakis, N., Damme, M. V., Ham, R. V., Visser, L., and Wolf, S., 2013. "Variable impedance actuators: a review". *Robotics and Autonomous Systems,* **61**, pp. 1601–1614.

[12] Song, S., She, Y., Wang, J., and Su, H.-J., 2020. "Toward tradeoff between impact force reduction and maximum safe speed: Dynamic parameter optimization of variable stiffness robots". *Journal of Mechanisms and Robotics,* **12**, p. 054503.

[13] Park, J.-J., Kim, H.-S., and Song, J.-B., 2009. "Safe robot arm with safe joint mechanism using nonlinear spring system for collision safety". pp. 3371–3376.

[14] Lee, W., Choi, J., and Kang, S., 2009. "Spring-clutch: A safe torque limiter based on a spring and cam mechanism with the ability to reinitialize its position". In 2009 IEEE/RSJ International Conference on Intelligent Robots and Systems, pp. 5140–5145.

[15] Lauzier, N., and Gosselin, C., 2011. "Series clutch actuators for safe physical human-robot interaction". In 2011 IEEE International Conference on Robotics and Automation, pp. 5401–5406.

[16] Kashiri, N., Laffranchi, M., Caldwell, D., and Tsagarakis, N., 2016. "Dynamics and control of an anthropomorphic compliant arm equipped with friction clutches". *IEEE/ASME Transactions on Mechatronics,* **21**(2), pp. 694–707.

[17] Niu, Z., Awad, M. I., Shah, U. H., Boushaki, M. N., Zweiri, Y., Seneviratne, L., and Hussain, I., 2022. "Towards safe physical human-robot interaction by exploring the rapid stiffness switching feature of discrete variable stiffness actuation". *IEEE Robotics and Automation Letters,* **7**(3), pp. 8084–80910.

[18] Ono, Y., Shimamoto, K., Nogawa, T., Masuta, H., and Lim, H.-O., 2013. "Passive collision force suppression mechanism for robot manipulator". pp. 280–285.

[19] Seriani, S., Gallina, P., Scalera, L., and Lughi, V., 2018. "Development of n-DoF preloaded structures for impact mitigation in cobots". *Journal of Mechanisms and Robotics,* **10**, p. 051009.

[20] Lauzier, N., and Gosselin, C., 2012. "Performance indices for collaborative serial robots with optimally adjusted series clutch actuators". *Journal of Mechanisms and Robotics,* **4**(2).

[21] Zhang, M., Laliberté, T., and Gosselin, C., 2016. "Design and static analysis of elastic force and torque limiting devices for safe physical human-robot interaction". In V05BT07A062, p. V05BT07A062.

[22] Zheng, Y.-F., and Hemani, H., 1985. "Mathematical modeling of a robot collision with its environment". *Journal of Robotic Systems,* **2**(3), pp. 289–307.

[23] Mills, J., and Nguyen, C., 1992. "Robotic manipulator collisions: Modeling and simulation". *Transactions of the ASME,* **114**, pp. 650–659.

[24] Aouaj, I., Padois, V., and Saccon, A., 2021. "Predicting the post-impact velocity of a robotic arm via rigid multibody models: an experimental study". pp. 2264–2271.

[25] Wang, Y., Dehio, N., and Kheddar, A., 2022. "On inverse inertia matrix and contact-force model for robotic manipulators at normal impacts". *IEEE Robotics and Automation Letters,* **7**, pp. 3648–3655.

[26] Park, J.-J., and Song, J.-B., 2009. "Collision analysis and evaluation of collision safety for service robots working in human environments". pp. 1–6.

[27] Haddadin, S., Krieger, K., Mansfeld, N., and Albu-Schäffer, A., 2012. "On impact decoupling properties of elastic

robots and time optimal velocity maximization on joint level". pp. 1–8.
[28] Lauzier, N., and Gosselin, C., 2015. "A comparison of the effectiveness of design approaches for human-friendly robots". *Journal of Mechanical Design,* **137**, pp. 1–8.
[29] Ostyn, F., Vanderborght, B., and Crevecoeur, G., 2022. "Overload clutch with integrated torque sensing and decoupling detection for collision tolerant hybrid high-speed industrial cobots". *IEEE Robotics and Automation Letters,* **7**, pp. 12601–12607.
[30] Kim, J., Cho, C., Song, J., Kim, Y., and Kyung, J., 2022. "Collision detection algorithm to distinguish between intended contact and unexpected collision". *Advanced Robotics,* **26**, pp. 1–16.
[31] Spong, M., Hutchingson, S., and Vidyasagar, M., 2005. *Robot Modeling and Control*. Wiley.
[32] Albu-Schäffer, A., 2001. "Regelung von robotern mit elastischen gelenken am beispiel der dlr-leichtbauarme".